Received: 23 February 2018 | Revised: 9 May 2018 | Accepted: 1 June 2018

DOI: 10.1002/mrm.27418

FULL PAPER

Magnetic Resonance in Medicine

Optimization of the spatial modulation function of vessel-encoded pseudo-continuous arterial spin labeling and its application to dynamic angiography

Yuriko Suzuki[1] | **Matthias J. P. van Osch**[1] | **Noriyuki Fujima**[2] | **Thomas W. Okell**[3]

[1]C.J. Gorter Center for High Field MRI, Department of Radiology, Leiden University Medical Center, Leiden, The Netherlands

[2]Department of Diagnostic and Interventional Radiology, Hokkaido University Hospital, Hokkaido, Japan

[3]Wellcome Centre for Integrative Neuroimaging, FMRIB, Nuffield Department of Clinical Neurosciences, University of Oxford, Oxford, United Kingdom

Correspondence
Yuriko Suzuki, Institute of Biomedical Engineering, University of Oxford, Old Road Campus, Headington, Oxford, OX3 7DQ, United Kingdom.
Email: yuriko.suzuki@eng.ox.ac.uk

Funding information
This research was supported by the EU under the Horizon2020 program (project: CDS-QUAMRI). T.O. is funded by the UK Royal Academy of Engineering. The Wellcome Centre for Integrative Neuroimaging is supported by core funding from the Wellcome Trust (203139/Z/16/Z).

Purpose: In vessel-encoded pseudo-continuous arterial spin labeling (ve-pCASL), vessel-selective labeling is achieved by modulation of the inversion efficiency across space. However, the spatial transition between the labeling and control conditions is rather gradual, which can cause partial labeling of vessels, reducing SNR-efficiency and necessitating complex postprocessing to decode the vessel-selective signals. The purpose of this study is to optimize the pCASL labeling parameters to obtain a sharper spatial inversion profile of the labeling and thereby minimizing the risk of partial labeling of untargeted arteries.

Methods: Bloch simulations were performed to investigate how the inversion profile was influenced by the pCASL labeling parameters: the maximum (G_{max}) and mean (G_{mean}) labeling gradient were varied for ve-pCASL with unipolar and bipolar gradients. The findings in the simulation study were subsequently confirmed in an in vivo volunteer study. Moreover, conventional and optimized settings were compared for 4D-MRA using four-cycle Hadamard ve-pCASL; the visualization of arteries and the presence of the partial labeling were assessed by an expert observer.

Results: When using unipolar gradient, lower G_{mean} resulted in a steeper spatial transition, whereas the width of the control region was broader for higher G_{max}. The in vivo study confirmed these findings. When using bipolar gradients, the control region was always very narrow. Qualitative comparison of the 4D-MRA demonstrated lower occurrence of partial labeling when using the optimized gradient parameters.

Conclusion: The shape of the ve-pCASL inversion profile can be optimized by changing G_{mean} and G_{max} to reduce partial labeling of untargeted arteries.

KEYWORDS
ASL-based 4D-MRA, vessel-encoded pCASL, vessel selective labeling

1 | INTRODUCTION

In the past decade, dynamic MRA (4D-MRA) using arterial spin labeling (ASL) has become an important alternative to contrast-enhanced (CE) 4D-MRA in the brain. The use of ASL for 4D-MRA has several advantages, which are not only its ability to visualize arteries without using contrast agent, but also fewer constraints on the attainable spatial and temporal resolution, because ASL does not need to capture the first-pass of the bolus (labeled blood) in real-time, unlike CE-4D-MRA. The ability to exclusively visualize the vascular tree arising from a selected artery by means of vessel selective labeling is an additional advantage of ASL-based MRA, which provides beneficial information for the diagnosis, treatment planning, and follow-up of many cerebrovascular diseases.[1,2]

Both pulsed-ASL (PASL) and pseudo-continuous ASL (pCASL) can provide vessel selective labeling, but their approaches are fundamentally different. In PASL, a spatially selective inversion slab is applied to the targeted artery or arteries, which is usually planned parallel to the arteries in the neck, so that the labeling pulse covers the target arteries over a long distance to label a sufficient amount of arterial blood.[2-4] The benefit of the PASL technique for selective labeling is a sharp profile of the labeling slab, which achieves clear selectivity of the targeted artery from untargeted arteries. However, to label as much arterial blood as possible, the labeling slab has to cover a large part of the target artery, which frequently results in erroneously inclusion of other, untargeted arteries, because of tortuous vascular anatomy.[5]

In contrast, in pCASL labeling of arterial blood is performed by means of flow-driven pseudo-adiabatic inversion in a thin labeling plane planned perpendicular to the flow direction. In vessel-encoded pCASL (ve-pCASL), additional gradients are applied in the in-plane (G_{xy}) direction, generating in-plane phase differences which produce a sinusoidal-like pattern of labeling and control conditions within the labeling plane.[6] These are used to label different combinations of arteries in a Hadamard-encoding scheme, allowing SNR-efficient calculation of individual vessel-selective images in postprocessing. Due to the thin labeling plane used, planning can be done with very little restrictions even when tortuous vascular anatomy is present in the inferior-superior direction.

When looking into more detail at the in-plane spatial modulation, however, it will be noted that the transition between the labeling and the control conditions is much more gradual than the PASL profile by, e.g., a hyperbolic secant or frequency offset corrected inversion (FOCI) pulse.[7,8] This more gradual transition could easily lead to partial labeling of untargeted arteries, leading to reduced SNR efficiency[6,9] and the requirement for complex postprocessing to separate out the individual contributions from each vessel. Previously, ve-pCASL with eight-cycled Hadamard encodings were presented for ve-4D-MRA of four arteries with relatively high spatial and temporal resolution.[10] For postprocessing, this study relied on Bayesian inference analysis to solve partial labeling of untargeted arteries.[11] When considering application in clinical protocols, the eight encodings and their associated long scan time of 18 min, would be an important hurdle for its use and would make the examination prone to artefacts due to subject motion.

In this article, we investigate how the in-plane spatial modulation of the vessel selective inversion labeling in ve-pCASL can be controlled by changing the labeling parameters such as the maximum (G_{max}) and mean (G_{mean}) labeling gradient strength, so that a sharper spatial modulation and broader, flatter control regions can be achieved. With these improvements, a more SNR-efficient encoding can be performed. Moreover, the sharper inversion profile and broader, flatter control regions could enable two or more spatially distinct arterial branches to be encoded in a near-identical manner, such that they can be treated as a single artery in the analysis, allowing a reduced number of vessel-encodings to be performed. To this end, first Bloch simulations are performed to elucidate the relationship between the shape of the inversion profile and the pCASL labeling parameters. Subsequently, these findings are validated in an in vivo study. Finally, the optimized inversion profile of the ve-pCASL sequence is applied to a 4D-MRA protocol[6] to demonstrate the ability to allow both vertebral arteries (VAs) to be encoded as a single entity, despite their spatial separation. This enables a three-vessel encoding scheme, which only requires four-cycled Hadamard-encodings,[12] thereby reducing the scan time by a factor of two compared with our previous sequence based on eight Hadamard-encodings.[10]

2 | METHODS

2.1 | Spatial modulation of ve-pCASL labeling

To devise a strategy for optimizing the inversion profile of ve-pCASL, we first revisit the mechanism which underlies this process and consider how it might be affected by various sequence parameters. For vessel selective labeling in ve-pCASL, additional gradients (G_{xy}) are applied in between the labeling RF pulses to generate in-plane phase differences. In one implementation G_{xy} is applied alternately positive and negative (Figure 1A),[6] whereas in another approach G_{xy} is not alternated (Figure 1B).[9] These two approaches will be subsequently referred to as the *bipolar approach* and *unipolar approach* throughout this article.

In such vessel selective approaches, the additional phase accrual due to G_{xy} is superimposed upon the phase accrual of

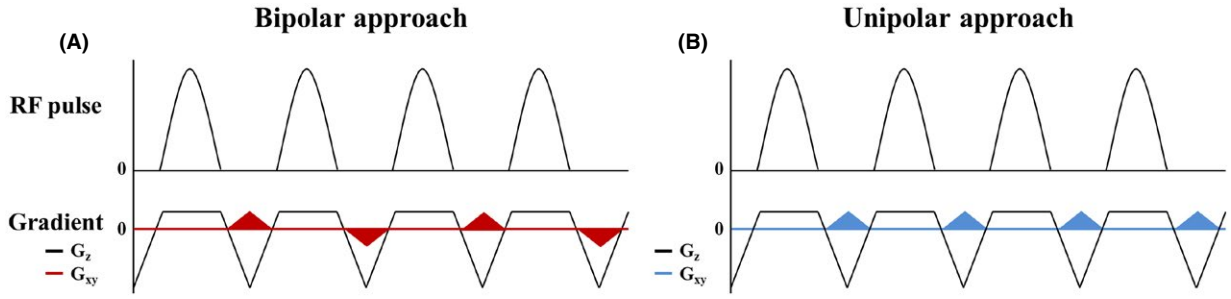

FIGURE 1 Schematic diagrams of pCASL labeling and additional gradients applied in the in-plane direction (G_{xy}), which are colored in red and blue, to achieve the spatial modulation. (A) In the bipolar approach, G_{xy} is applied alternately positive and negative. (B) In the unipolar approach, G_{xy} is always played out with the same polarity

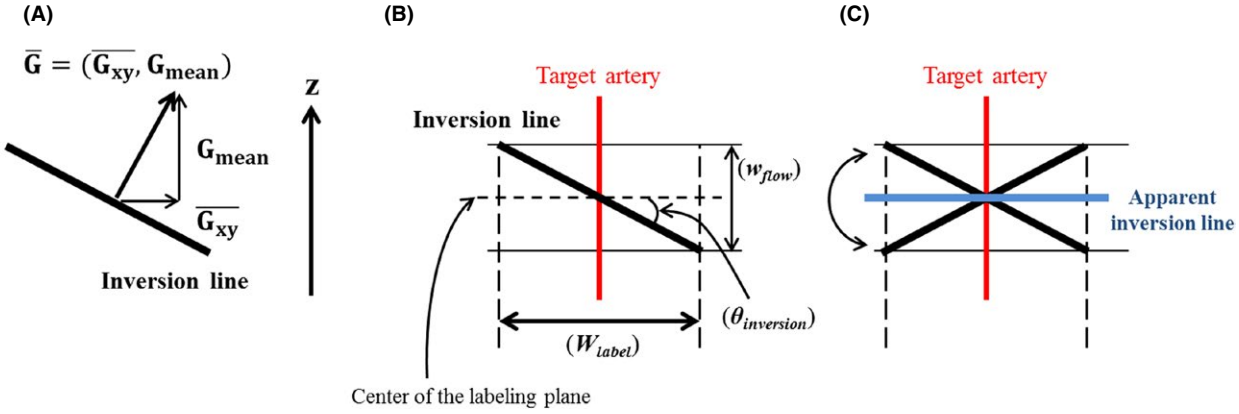

FIGURE 2 Schematic drawings illustrating: the "inversion line," which is determined by the two orthogonal gradients G_{mean} and $\bar{G}_{xy}$ (A); "w_{flow}", indicating the distance over which adiabatic inversion occurs in the flow direction; "$\theta_{inversion}$", the angle between the inversion line and the labeling plane; and "W_{label}", which represents the width of the labeling condition for vessel selective labeling (B). (C) In the bipolar approach, the inversion line is flipped every other G_{xy}, resulting in an averaged inversion line parallel to the labeling plane

the flowing blood due to the nonzero mean gradient in the z-direction (G_{mean}) that produces the flow-driven pseudo-adiabatic inversion in pCASL. The inversion of the flowing blood magnetization will occur, therefore, where the additional net phase accrual due to G_{xy} is close to zero or multiples of 2π (with respect to the pCASL RF pulses), whereas the control condition is produced when this additional phase is in the opposed direction (with π shift). This results in a repeating pattern of labeling and control conditions across the labeling plane.

What has not previously been considered, to the best of our knowledge, is the interaction between phase-accruals of the G_{xy} and G_{mean} gradients, both in the xy-plane as well as in the z-direction. In the unipolar approach the consistent application of two orthogonal gradients (G_{mean} and G_{xy}) means that the center of the inversion (where the net phase accrual is zero or a multiple of 2π) occurs on a series of tilted lines ("inversion lines"), as Figure 2A shows. The effective width where adiabatic inversion is performed in the flow direction ("w_{flow}" in Figure 2B) is determined by the gradient strength as used during the pCASL labeling (commonly known as G_{max}) in combination with the bandwidth of the RF pulses. The angle between the inversion line and the labeling plane ("$\theta_{inversion}$" in Figure 2B) will be determined by the relative strengths of G_{mean} and the time-averaged G_{xy} gradient ($\bar{G}_{xy}$).

Because it can be presumed that the flow-driven adiabatic inversion only occurs if blood water passes through an inversion line within the width of w_{flow}, the width of "W_{label}" in Figure 2B, which represents the in-plane width of labeling condition for vessel selective labeling, will be dependent on G_{max}, G_{mean}, and G_{xy}. In contrast, for the bipolar approach, no consistent inversion line is created due to the alternating G_{xy} gradient, as illustrated in Figure 2C. Instead, alternating G_{xy} gradient prevent the continuous accumulation of additional phase due to G_{xy} at off-center locations, thereby resulting in an apparently untilted inversion lines.

2.2 | Bloch equation simulations

The inversion profile of ve-pCASL was investigated by Bloch equation simulations performed in MATLAB (Mathworks, Natick, MA). The pCASL labeling parameters were varied to allow the identification of an optimal inversion profile shape with a sharp transition between labeling and control conditions. With both unipolar and bipolar approaches, the longitudinal magnetization (M_z) was simulated in two directions: first in the flow-direction to observe the temporal evolution of the adiabatic inversion, and, second, in the direction of G_{xy} to observe the resultant spatial modulation of the inversion. The shape of inversion profile was obtained at downstream from the center of inversion ($z = 0$) at a distance approximately equivalent or greater than half of w_{flow}, ensuring that the M_z curves were stabilized at that point. The simulation was performed with flow velocities of 5, 10, 20, 30, 40, 50, and 60 cm/s.

For the calculation of the inversion profile, M_z from all flow velocities were incorporated, assuming a laminar flow profile. For simplicity it was assumed that G_{xy} was applied only in the x-direction. The amplitude of G_{xy} was chosen to achieve a distance of 50 mm between the center of labeling and control conditions. Moreover, it was assumed that for on-resonance spins the center of the labeling condition occurs at the iso-center ($x = 0$). Parameters for pCASL labeling were set as follows: G_{max} of 6.0 mT/m, G_{mean} of 0.8 mT/m, pCASL labeling RF pulse duration of 0.6 ms, interval of 1.0 ms and flip angle of 20º (similar to Okell et al),[13] and this set of parameters will be referred to as the *default settings*. Subsequently, G_{max} was varied from 7.0 mT/m to 2.0 mT/m in steps of 1.0 mT/m and G_{mean} was varied from 0.9 mT/m to 0.2 mT/m with 0.1-mT/m intervals. A longer RF pulse interval of 1.2 ms, and different flip angles of 17º and 23º were also simulated. T_2 of blood was assumed to be 200 ms and T_1 recovery was neglected.[6,14]

2.3 | In vivo healthy volunteer study

Following the simulation study, two in vivo volunteer studies were conducted (i) to validate the spatial modulation of the inversion as observed in the simulation study, and (ii) to demonstrate the potential improvement of ve-pCASL 4D-MRA when using the selected optimal settings. All scans were performed on a Siemens 3T TIM Verio (Siemens Healthineers, Erlangen, Germany) under a technical development protocol agreed by local ethics and institutional committees. A total of six volunteers (female = 3, mean age = 36 years [range, 27-46 years]) without known cerebrovascular disease participated in the studies, in which one participated only in study-(i), one participated in both studies, and the other four volunteers participated only in study-(ii).

2.4 | Validation of the inversion spatial modulation

To validate the inversion profile vessel selective labeling was performed within a labeling plane approximately 8 cm below the circle of Willis, through the proximal V3 segment of the vertebral arteries (VAs), where the internal carotid arteries (ICAs) and VAs form an approximately rectangular arrangement. The transverse gradient (G_{xy}) was applied in the right-left (RL) direction with the amplitude corresponding to a π phase difference between the right ICA (RICA) and left ICA (LICA). The center of the selective labeling was first located at the RICA (i.e., the center of the control condition at the LICA) and was subsequently shifted toward the LICA in steps of 2 mm until the center of labeling condition reached the LICA (at the same time, the RICA will experience the center of the control condition). At each offset, two acquisitions were performed with an alternating π-phase difference of the labeling RF-pulse train for the second acquisition, which effectively swaps the location of the control and labeling condition. Additionally, a pair of nonselective labeling and control conditions was acquired.

To simplify the postprocessing and to keep the total examination time reasonably short, a low spatial resolution perfusion readout sequence (multi-slice single-shot echo planar imaging) was used, instead of a high-resolution 3D-MRA acquisition. The labeling duration and postlabeling delay were set to shorter values than typical for perfusion imaging (1400 and 1000 ms, respectively) to boost the SNR and keep the examination time short, thereby reducing the risk of subject motion.

Following the results of the Bloch equation simulations (see the Results section), the unipolar approach was adopted and two combinations of G_{max} and G_{mean} were compared with the default settings (as defined in the simulation study): new setting-(A): G_{max} of 6.0 mT/m and G_{mean} of 0.4 mT/m, and new setting-(B): G_{max} of 3.0 mT/m and G_{mean} of 0.2 mT/m. All other parameters were kept equal to the default settings.

Other perfusion imaging parameters were as follows: FOV 220 × 220 mm, scan matrix 64 × 64, 4.5 mm slice thickness, 22 slices, TE/TR of 14/3440 ms. A WET presaturation scheme was inserted before labeling,[3,15] and two nonselective hyperbolic secant inversion pulses were applied during the postlabeling delay for background suppression. The number of offset steps from RICA to LICA varied depending on the distance between them: 27 and 24 steps for volunteer 1 and 2, respectively, which resulted in an average scan time of approximately 3 min for each setting of labeling parameters.

To measure the perfusion signal arising from the RICA and LICA separately, masks for the vascular territories were generated from a separate ve-pCASL scan acquired with eight Hadamard-encodings, as previously described.[16] Using

these masks, the mean signal intensity of each perfusion territory was measured for each offset, and they were normalized to values using nonselective labeling and control images as follows:

$$\textit{Normalised signal} = -\left(\frac{\textit{nonselective control}-\textit{selective labeling}}{\textit{nonselective control}-\textit{nonselective labeling}}\right). \quad (1)$$

This suggests that perfect control or inversion will yield a values of 0 or -1, respectively. Finally, the normalized inversion profile curves were plotted as a function of the offset.

2.5 | ve-pCASL 4D-MRA

To demonstrate the potential improvements achievable with the two newly proposed settings (A and B) compared with the default settings, 4D-MRA images were acquired in five subjects by means of a three-vessel encoding scheme with four Hadamard-encodings (previously proposed by Günther using a PASL labeling module).[12] Although labeling is performed at the level in the neck where the two VAs are widely separated (Figure 3A), the newly proposed parameter settings with the benefit of broader, flatter control regions allows us to treat both VAs as a single artery. On the time-of-flight image acquired before the 4D-MRA scan, the coordinate of the center of each artery was obtained, which was used to determine the distance between the center of the labeling and control conditions, as well as the direction of the G_{xy} gradient. The labeling was performed as follows: 1st cycle, label condition at RICA; 2nd cycle, label condition at LICA; 3rd cycle, label condition at both VAs (see Figure 3B); and 4th cycle, label condition for all arteries (nonselective). The measured signal **y** can subsequently be written as follows:

$$\mathbf{y} = \begin{pmatrix} -1 & 1 & 1 & 1 \\ 1 & -1 & 1 & 1 \\ 1 & 1 & -1 & 1 \\ -1 & -1 & -1 & 1 \end{pmatrix} \begin{pmatrix} RICA \\ LICA \\ VAs \\ S \end{pmatrix} \quad (2)$$

where S is static tissue. By applying the pseudo-inverse matrix of Equation (2), vessels supplied by each feeding artery are visualized separately. For an optimal encoding function both VAs need to be placed equally well in the label or control conditions across all encoding cycles, allowing them to be treated as a single artery for the analysis. This will optimise SNR-efficiency and allowing the simple form of the Hadamard-matrix (Equation (2) above) to be used to decode the data without having to account for partial labeling of arteries in one or more encoding cycle. In this study, a 5th cycle consisting of a nonselective control condition was also added to allow the calculation of a nonselective 4D-MRA subtracted image for comparison, as described below.

The same three parameter settings using the unipolar approach were used as in study-(i), i.e., the default settings, new setting-(A) and -(B). The pCASL labeling duration was set to 500 ms, and a 4D SPGR Look-Locker[13,17] readout module was performed immediately after the end of labeling, in which five phases were acquired with a temporal resolution of 166.7 ms. Acquisition parameters for the 4D SPGR were as follows: FOV 200 × 200 mm, scan matrix 192 × 192, in-plane GRAPPA factor 4, 30 slices with a thickness 2.0 mm, readout excitation flip angle 7°, TR 9.3 ms, TE 4.9 ms. The scan time was 7 min 12 s for four encoding cycles (9 min including the nonselective control acquired for comparison).

From the decoded vessel-selective datasets (generated by applying the pseudo-inverse matrix of Equation (2) to the images from the first four encoding cycles) and noselective datasets

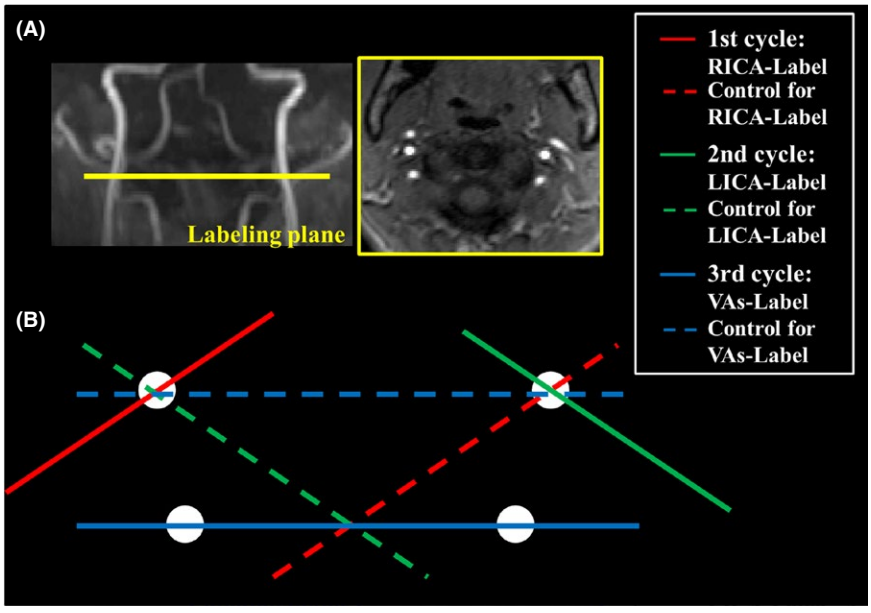

FIGURE 3 (A) Illustration of the planning of the pCASL labeling plane on the coronal and transverse angiography surveys. (B) Schematic figure illustrating the planning for the vessel-selective labeling of 1st (RICA-label), 2nd (LICA-label) and 3rd cycle (VAs-label). Red, green, and blue colors indicate the 1st, 2nd, and 3rd cycle. The dashed lines indicate the center of control condition of each cycle

(from the subtraction of nonselective label and control cycles only), maximum intensity projection images were generated in the sagittal, transverse and coronal directions. A qualitative comparison among the three different parameter settings based upon the overall image quality and the degree of partial labeling of untargeted arteries was performed by a neuroradiologist with 13 years of experience (N.F.). The visual scoring system was as follows: For nonselective 4D-MRA: (a) Clear visibility of posterior communicating (p-com) arteries (yes/no); (b) Visualization of arteries (3, good; 2, moderate; 1, very poor). For ve-4D-MRA: (c) Presence of partial labeling of untargeted arteries (3, not observed; 2, slightly present; 1, very obviously present); (d) Visualization of arteries (3, good; 2, moderate; 1, very poor).

3 | RESULTS

3.1 | Bloch equation simulations

Figure 4 shows color-coded 2D maps of M_z in the flow-direction (from the bottom to the top of the images) and in the direction of G_{xy} (left-right in the images) for the unipolar approach (Figure 4A) and bipolar approach (Figure 4B), respectively. As a representative example, only data simulated with a flow velocity of 30 cm/s is shown. The predicted tilted inversion line for the unipolar approach (see Figure 2B) was confirmed, as can be concluded from Figure 4A by looking at the tilted transition line between before (in red) and after inversion (in blue). As hypothesized, a smaller G_{max} indeed led to a wider w_{flow}, whereas a smaller G_{mean} produced steeper $\theta_{inversion}$.

For bipolar gradients, in contrast, the inversion line was parallel to the pCASL labeling plane as also hypothesized by the averaging effect of the alternating G_{xy}, as illustrated in Figure 2C. In Supporting Information Figure S1, color-coded 2D maps obtained by the unipolar approach with flow velocities of 10 cm/s (Supporting Information Figure S1A) and 50 cm/s (Supporting Information Figure S1B) are shown. As shown in the original ve-pCASL article by Wong[6] (Figure 2b), the spatial modulation of the inversion (i.e., M_z in the x-direction) is influenced by flow velocity. In 2D maps with different flow velocities of 10 cm/s (Supporting Information Figure S1A), 30 cm/s (Figure 4A) and 50 cm/s (Supporting Information Figure S1B), a difference of the transition between the labeling to the control conditions in the direction of G_{xy} was notable.

However, the same trends as for 30 cm/s were observed between G_{max} and w_{flow}, as well as between G_{mean} and $\theta_{inversion}$. Additionally, color-coded 2D maps obtained with stronger G_{xy} to achieve a distance of 15 mm between the center of labeling and control conditions, which is approximately the anterior-posterior distance between the ICAs and VAs, are shown in Supporting Information Figure S2. This figure suggests that the narrower setting to achieve anterior-posterior discrimination between the ICAs and VAs results in a very narrow labeling condition, which could cause suboptimal labeling as also seen in the in vivo study (see the Discussion section), although the modulation patterns are proportionally identical to the ones with 50 mm distance.

At the center of the label condition in the x-direction (i.e., at the center of the targeted artery), flow-driven adiabatic inversion showed slightly different evolution for different G_{max} and G_{mean} settings: with fixed G_{mean} (Figure 5A), inversion started and ended further from the labeling plane when G_{max} was lower, which reflects the thickness of the pCASL labeling plane. Note that the trajectory of M_z close to the middle of the labeling plane (i.e., when M_z is crossing 0) was very similar for all G_{max} values (indicated by an arrow in Figure

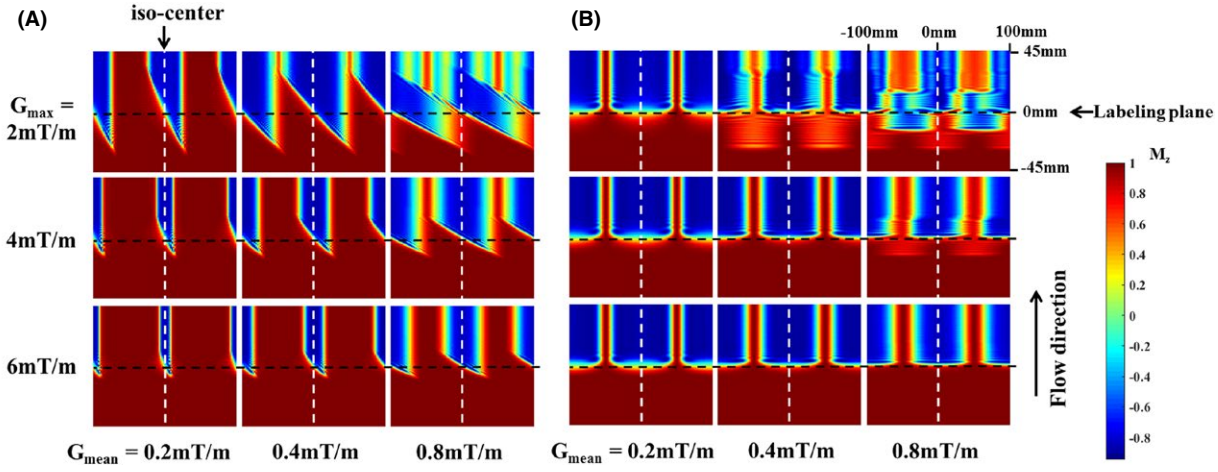

FIGURE 4 Color-coded 2D maps of the simulated M_z as a function of distance in the direction of G_{xy} (left-right in these images) and in the flow-direction (bottom to top), using the unipolar approach (A) and the bipolar approach (B) for a range of G_{max} and G_{mean} values. Red and blue colors show the uninverted and inverted magnetization, respectively. As a representative example, only data simulated with a flow velocity of 30 cm/s is shown

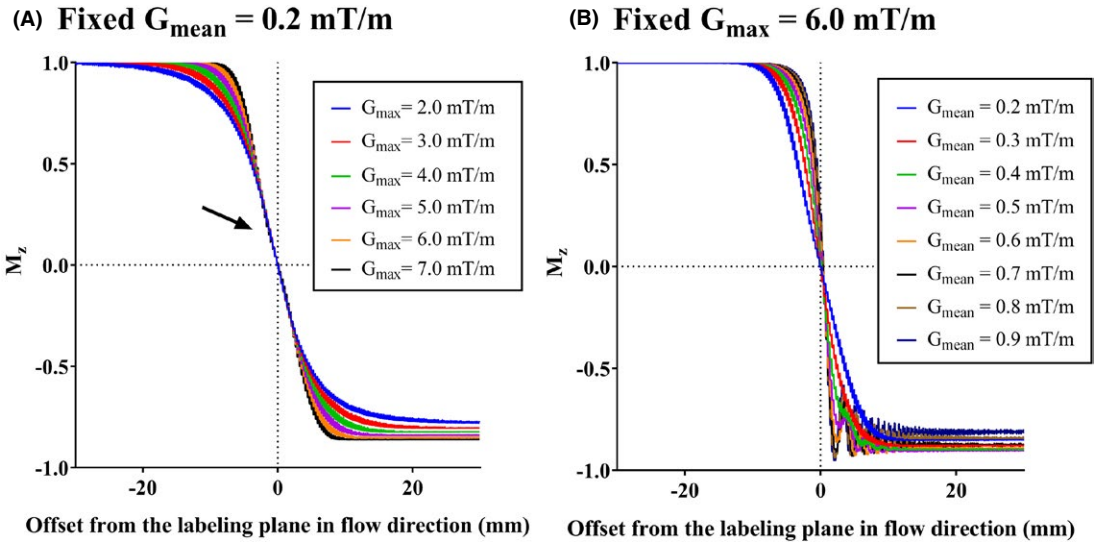

FIGURE 5 Simulated M_z showing the evolution of the flow-driven pseudo-adiabatic inversion at the location of the targeted artery (isocenter), with fixed G_{mean} and variable G_{max} (A), and fixed G_{max} and variable G_{mean} (B). As a representative example, only data simulated with a flow velocity of 30 cm/s is shown

5A). In contrast, higher G_{mean} resulted in faster inversion when G_{max} was kept constant (Figure 5B).

Figure 6 shows representative spatial modulation of the inversion as obtained with the bipolar (Figure 6A,B) and unipolar approach (Figure 6C,D). For the bipolar approach, the control condition (indicated by arrows) was very narrow for all studied combinations of G_{max} and G_{mean}, which was considered sub-optimal for the purpose of this study. Therefore, further in vivo studies were only performed using the unipolar approach, which does allow tuning the width of the control condition. When using the unipolar approach, flat control regions were obtained over a wide distance for many combinations of G_{max} and G_{mean} (Figure 6C,D). As Figure 6C shows, the steepness of the inversion profile was similar for all G_{max} when G_{mean} was kept constant (at 0.2 mT/m in Figure 6C), whereas larger G_{max} resulted in a narrower labeling condition and wider control condition. In contrast, with fixed G_{max} (at 6.0 mT/m in Figure 6D) lower G_{mean} resulted in a steeper inversion profile.

As Figure 7A indicates, when G_{max} is small and/or G_{mean} is large (i.e., a small ratio of G_{max}/G_{mean}), the control condition becomes very narrow and with an even smaller ratio of G_{max}/G_{mean} the shape of inversion profile starts to become irregular. In such settings, disturbances were also observed during the flow-driven adiabatic inversion (Figure 7B, G_{max} = 2.0 mT/m and G_{mean} = 0.8 mT/m at flow velocity of 30 cm/s). With the same combination of G_{max} and G_{mean}, Figure 4A (upper right) shows overlapping of tilted inversion lines, from which it can be deduced that the magnetization experiences multiple inversion planes, leading to highly irregular behavior.

Spatial modulations produced with different pCASL flip angles of 17° (Supporting Information Figures S3B and S4B) and 23° (Supporting Information Figures S3C and S4C) resulted in slightly lower and higher inversion efficiencies for some combinations of G_{max} and G_{mean}, but in general the results are very similar. Also, a longer RF interval of 1.2 ms (Supporting Information Figures S3D and S4D) caused only slightly reduced inversion efficiency for some combinations of G_{max} and G_{mean}. However, none of these changes in RF pulse parameter settings caused important changes to the inversion profiles. Based on the results from the simulation studies, for the in vivo studies two combinations of G_{max} and G_{mean} were selected: (A) G_{max} = 6.0 mT/m, G_{mean} = 0.4 mT/m and (B) G_{max} = 3.0 mT/m, G_{mean} = 0.2 mT/m using the unipolar approach.

The setting-(B) was chosen because (i) the lowest G_{mean} = 0.2 mT/m resulted in the sharpest transition between the labeling and the control conditions, and (ii) a G_{max} higher than 3.0 mT/m resulted in too narrow labeling conditions as compared with the control condition. The setting-(A) was chosen because the combination of G_{max} = 6.0 mT/m and G_{mean} = 0.4 mT/m generates a similar shape of the inversion profile to the setting-(B) (see Figure 8A) while using the same G_{max} as the default setting. This allowed the investigation of whether a lower G_{max} in the setting-(B) (which generates the wider "w_{flow}") might introduce adverse effects on the inversion profile in in vivo studies, due to the greater likelihood of non-straight vessels within a broader labeling region. RF pulse duration and interval, as well as the flip angle were kept equal to the default setting (respectively, 0.6 ms, 1.0 ms, and 20º, see Figure 8A).

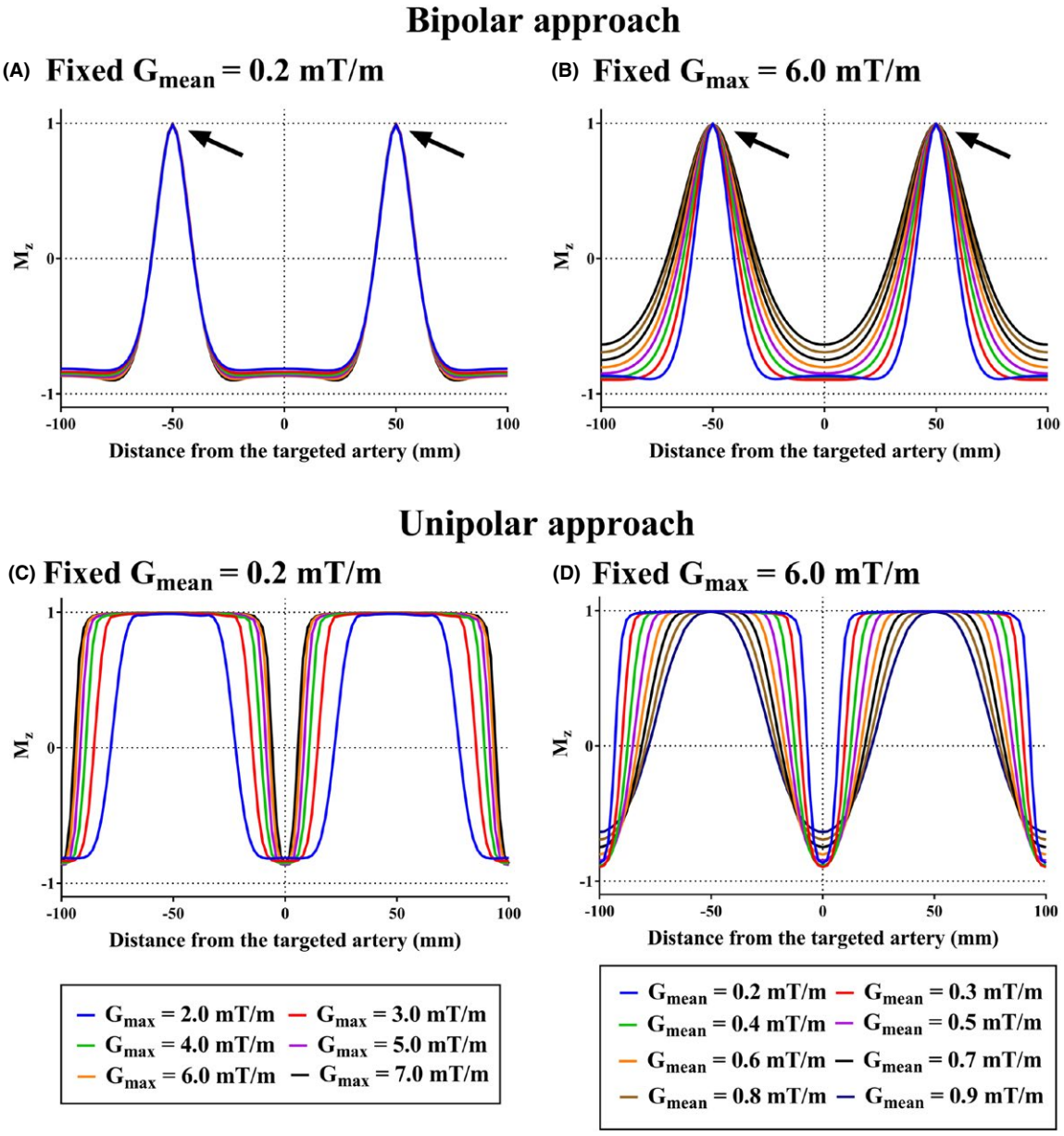

FIGURE 6 Simulated inversion profile curves (M_z as a function of distance along x), which were obtained downstream from the center of inversion (z = 0) at a distance approximately equivalent or greater than half of w_{flow}. (A) Bipolar approach, variable G_{max} and fixed G_{mean} at 0.2 mT/m. (B) Bipolar approach, fixed G_{max} at 6.0 mT/m and variable G_{mean}. (C) Unipolar approach, variable G_{max} and fixed G_{mean} at 0.2 mT/m. (D) Unipolar approach, fixed G_{max} at 6.0 mT/m and variable G_{mean}. Black arrows indicate the very narrow control condition obtained with the bipolar approach across all gradient settings

3.2 | In vivo healthy volunteer study

3.2.1 | Validation of the inversion spatial modulation

Figure 8B shows the inversion profile curves measured from both volunteers. These plots show the normalized inversion of the mean signal from the RICA and LICA perfusion territories as a function of the vessel selective labeling offset from the target artery. Although some small signal offsets, due to scanner drift across the experiments, and minor shifts in the curves, due to possible off-resonance effects, were evident, sharper inversion profiles were clearly observed in both volunteers for the new settings as compared with the default settings.

3.3 | ve-pCASL 4D-MRA

Representative ve-4D-MRA images from one of the healthy volunteers are shown in Figure 9. (In Figure 9, only representative single phase is shown. For all five phases from this volunteer, and representative single phase from all five

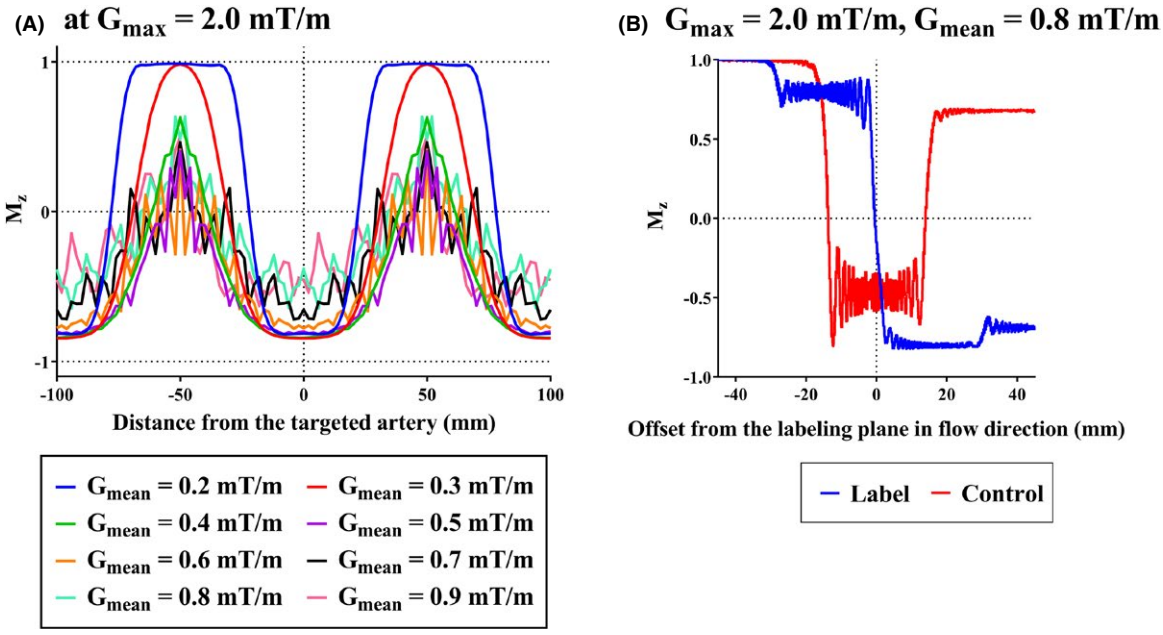

FIGURE 7 (A) The inversion profile curves (M_z as a function of location along x) simulated with small G_{max} and large G_{mean} (i.e., small ratio of G_{max}/G_{mean}), generating irregular shapes of the inversion profile. (B) The evolution of flow-driven pseudo-adiabatic inversion simulated with G_{max} = 2.0 mT/m and G_{mean} = 0.8 mT/m at flow velocity of 30 cm/s, showing the disturbance of inversion

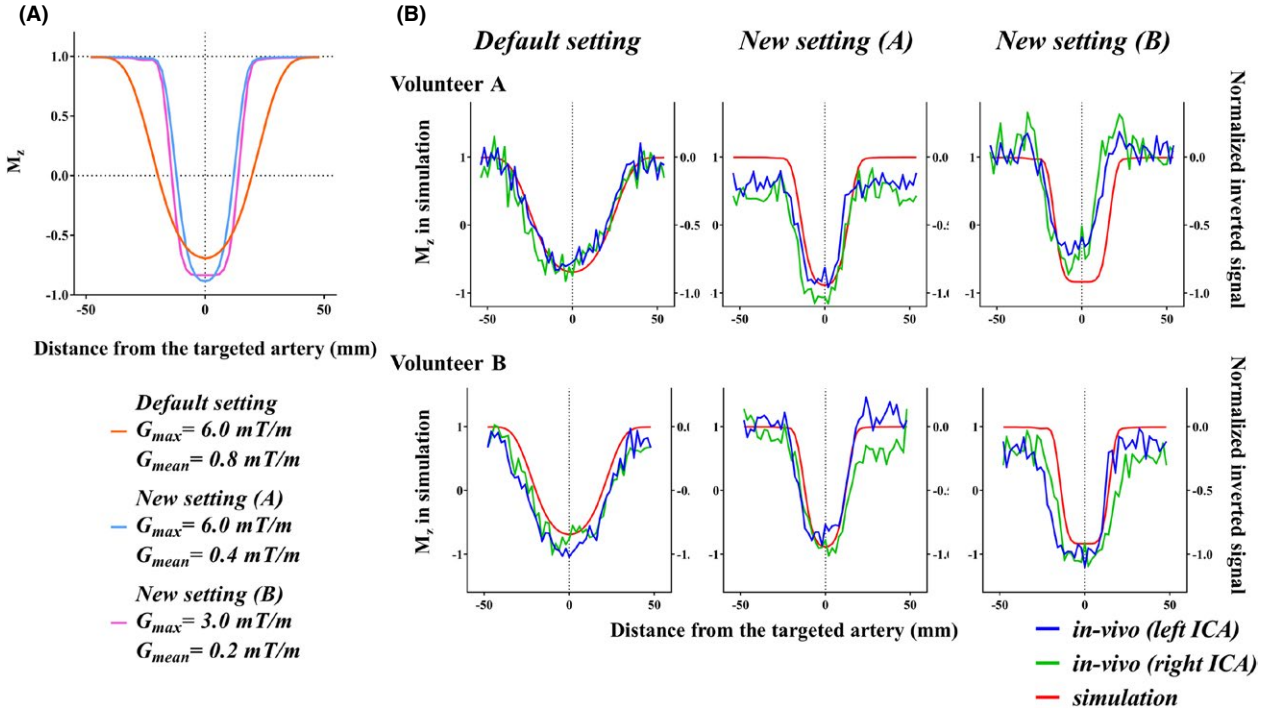

FIGURE 8 (A) The inversion profile curves simulated with the default setting G_{max} = 6.0 mT/m, G_{mean} = 0.8 mT/m and two new settings (New setting A) G_{max} = 6.0 mT/m, G_{mean} = 0.4 mT/m and (New setting B) G_{max} = 3.0 mT/m, G_{mean} = 0.2 mT/m, which were used for further in vivo studies, and (B) the inversion profile curves measured from two volunteers

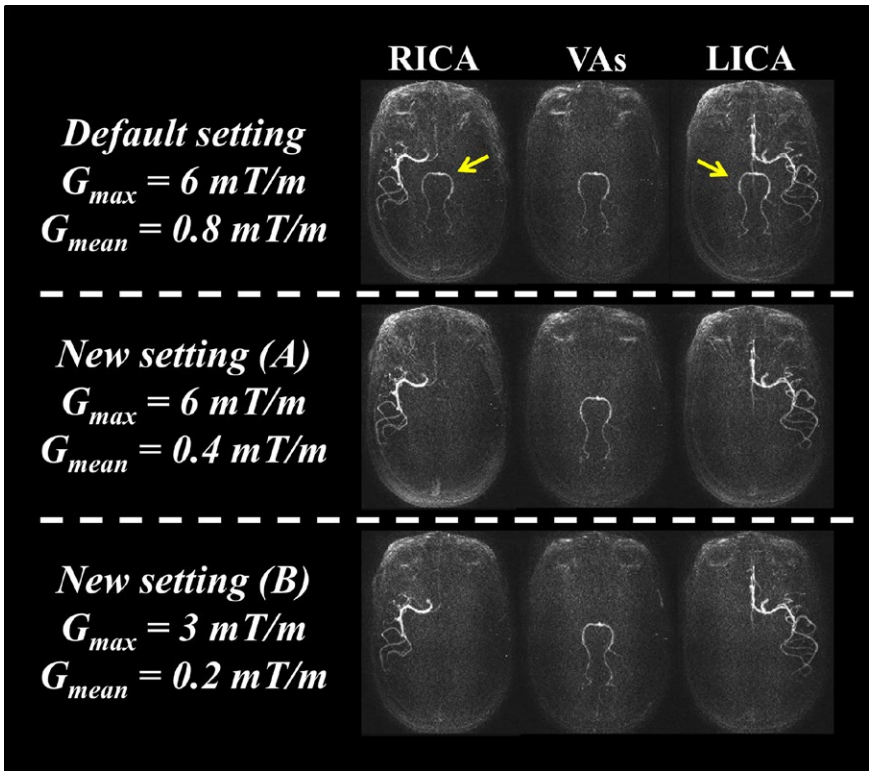

FIGURE 9 Representative ve-pCASL 4D-MRA images from one healthy volunteer acquired using the default settings (G_{max} = 6.0 mT/m, G_{mean} = 0.8 mT/m), the new setting (A) (G_{max} = 6.0 mT/m, G_{mean} = 0.4 mT/m), and new setting (B) (G_{max} = 3.0 mT/m, G_{mean} = 0.2 mT/m). Only representative single phase is shown. Yellow arrows indicate the partial labeling of untargeted arteries observed with the default setting which were not evident with both optimized settings

volunteers, see Supporting Information Figures S5 and S6, respectively.) The mean distance between RICA and LICA and between ICAs and VAs (which was represented as the distance between each central location of ICAs and VAs) were 53.6 and 12.3 mm, respectively. When using the default settings, partial labeling of VAs was observed as indicated by arrows. With both of the proposed new settings, however, no partial labeling could be observed and a clear separation was achieved for all targeted arteries, despite the separation of the VAs within the labeling plane.

The summary of the observer study is shown in Table 1. Although the flow through the p-com was visualized in two out of the five volunteers, the visualization of untargeted arteries due to the partial labeling could be distinguished from it. In RICA and LICA labeling, the default settings resulted in more frequent and severe partial labeling than when using the new settings. Statistical comparison by means of a paired t-test between the default (mean value of 2.13) and both new settings combined (mean value of 2.67) showed that this difference was statistically significant ($P < 0.005$). These results suggest that the sharper inversion profile indeed reduced the occurrence of partial labeling of untargeted arteries.

In ve-4D-MRA, slightly lower signal intensity was observed in the posterior cerebral arteries (PCAs) when using the new settings in some of the volunteers, although statistical comparisons of the mean visual scores by means of paired t-tests between the default and both new settings combined did not result in statistical significance for any arterial territory: 3.0 versus 3.0 (p = N/A) for RICA, 2.8 versus 3.0 (p = 0.168) for LICA, and 2.6 versus 2.2 ($P = 0.104$) for VAs. For the nonselective 4D-MRA, however, such a lower intensity as compared to the default setting was not observed, which suggests that this observation cannot be attributed to a decrease in the labeling efficiency due to the new settings. We refer to the discussion section for possible explanations.

4 | DISCUSSION

In this study, we have presented how the in-plane spatial modulation of ve-pCASL can be controlled by changing the labeling parameters, G_{max} and G_{mean}. By optimization, a sharper spatial modulation and broad, flat control regions were achieved, which allowed us to treat spatially distinct vessels, like the two VAs, as one single artery. This allowed us to use a three-vessel four-cycle Hadamard-encoding for 4D-MRA acquisition, which halved the scan time from our previous four-vessel eight-cycle Hadamard-encoding 4D-MRA.

From the Bloch equation simulation studies, three major observations can be made. First, for the unipolar approach, a flat control condition was obtained over a wide distance, whereas the bipolar approach produced a narrow control condition, which was considered suboptimal for the purpose of this study. The difference between these two approaches can be attributed to the angulation of the inversion line: for the bipolar gradients the inversion line is flipped every other

TABLE 1 Summary of the qualitative scoring of ve-pCASL 4D-MRA, using the default setting (G_{max} = 6.0mT/m, G_{mean} = 0.8mT/m), the new setting (A) (G_{max} = 6.0mT/m, G_{mean} = 0.4mT/m) and (B) (G_{max} = 3.0mT/m, G_{mean} = 0.2mT/m)

For non-selective 4D-MRA				
(a) Clear visibility of p-com arteries	Number of subjects			
	2			
(b) Visualization of arteries	Parameter setting	Mean score		
	Default	3.0		
	New (A)	3.0		
	New (B)	3.0		
For ve-pCASL 4D-MRA				
	Parameter setting	RICA	LICA	VAs
(c) Presence of partial labelling of untargeted arteries	Default	1.4	2.0	3.0
	New (A)	2.4	2.8	3.0
	New (B)	2.4	2.8	2.6
(d) Visualization of arteries	Default	3.0	2.8	2.6
	New (A)	3.0	3.0	2.4
	New (B)	3.0	3.0	2.0

G_{xy}, which prevents additional cumulative phase accruals due to G_{xy} at off-center locations. This appears to result in the inversion being achieved over relatively wide region until the alternation of G_{xy} starts to behave as an alternating π phase shift, thereby generating the control condition. It also explains why settings with different G_{max} in combination with fixed G_{mean} generate very similar spatial inversion modulations, while keeping the pointed narrow control condition.

Second, in unipolar approach a higher G_{max} produced a narrower region for the labeling condition with a wider control condition, while keeping the spatial transition between the labeling and control conditions similar for all G_{max}. From the schematic depiction of Figure 2, a lower G_{max} and thus a larger thickness of the pCASL labeling pulse will result in a wider w_{flow}, which was indeed observed as the wider inversion range for the M_z in the flow direction (see Figure 4A), whereas the angle of the tilted inversion line ("$\theta_{inversion}$" in Figure 2A) was constant for all G_{max}. It is, therefore, to be expected that a smaller G_{max} with wider w_{flow} result in a wider label condition ("W_{label}" in Figure 2A). Third, and finally, a smaller G_{mean} results in a steeper transition between labeling and control conditions, which can be explained by the following fact: the tilted inversion line indicates the center of the pseudo-adiabatic inversion in the flow-direction (i.e., where M_z crosses 0). When this line is not parallel to the labeling plane, this inversion center will shift from the center of the labeling plane along the flow-direction as a function of the offset from the target artery in the x-direction. When the center of adiabatic inversion occurs too close to the edge of w_{flow}, the adiabatic inversion starts to fail because the spins are no longer effectively tipped by the slice-selective pCASL pulse. In other words, the spins have left the labeling slab before full inversion has been achieved. A lower G_{mean} increases the angle of the inversion line, thereby resulting in a failure to achieve full inversion closer to the targeted artery, i.e., resulting in a steeper spatial transition.

For vessel-selective ASL imaging, the simplest approach is to perform a pair-wise labeling and control acquisition for a single targeted artery.[1,2,4] When all major arteries (RICA, LICA, and VAs) would be acquired in such a manner, however, the paired acquisitions of labeling and control conditions would require six acquisitions and, therefore, take considerable scan time. Therefore, several more time-efficient approaches have been proposed: for example, the dual-vessel labeling scheme of Zimine et al[5] in which each of the ICA and both of VAs are labeled simultaneously and, after subtraction from each control image, arterial signal from each ICA is isolated by assigning ASL signal present in both images as arterial blood originating from the VAs. Therefore, the total scan time for all major arteries will only be two-thirds of the one-by-one acquisition, although special care is needed to judge whether signal is from the VAs or could also be due to actual mixing of blood from both ICAs.

Such a risk of misinterpretation can be avoided by using a Hadamard-encoded ve-ASL scheme as proposed by Günther for PASL (12) and Wong for pCASL.[6] This is

a highly efficient approach for perfusion imaging in which repeated measurements for signal averaging can be replaced by multiple Hadamard-encodings without loss in SNR, i.e., vessel-encoding is done without a time penalty because an equal number of raw images are used to generate the perfusion images. However, such a free-lunch benefit is not possible for a 4D-MRA acquisition, because ASL-based MRA usually relies on a 3D multi-shot readout with a high spatial resolution, and the entire scan time is spent for spatial encoding, rather than averaging. Therefore, scan time for ve-4D-MRA would increase proportionally to the number of applied vessel-encodings as compared to a nonselective 4D-MRA scan.

In this study, we used a three-vessel encoding scheme, which only requires four Hadamard-encodings. However, such a scheme requires both VAs to behave as a single artery, necessitating stricter planning of labeling and especially a broad, flat control region to avoid partial labeling of one of the two spatially separated VAs. By using the sharper ve-pCASL inversion profile with the broader control regions as found in our simulation study, partial labeling of untargeted arteries could be minimized, thereby allowing the Hadamard-four scheme without having to account for partial labeling in postprocessing. This halved the scan time compared with our previous study using eight Hadamard-encodings of four arteries.[10]

An alternative approach would be to account for the occurrence of partial labeling, by including the nonideal inversion efficiency for each artery at each vessel-encoding cycle into the postprocessing, for example by applying a Bayesian analysis approach.[11] It should be noted, however, that presence of partial labeling reduces SNR-efficiency even though such a sophisticated analysis might enable proper vessel differentiation.

There are several limitations in this study. First, as the observer study shows, slightly lowered signal intensity was observed in the PCAs of some of volunteers, more frequently when using the new settings. Because the accompanying nonselective 4D-MRA image acquired with the same settings for pCASL-labeling did not show decreased signal intensity compared with the default settings, the possibility of a globally lowered labeling efficiency can be ruled out. The lower intensity is presumed to be caused by suboptimal labeling of the targeted arteries (VAs), possibly due to the narrower labeling condition as present with the optimized settings.

In this study, the center of each artery was measured on the time-of-flight image before the 4D-MRA scan, and the distance between those arteries was used to determine the distance between the center of the labeling and control conditions. This last distance also determines the width of the label and control regions. Because the distance between ICAs and VAs was often quite small, this also might have caused the labeling condition to become too narrow to effectively cover both VAs. However, this study has shown that the control condition can be much wider and flatter by using the newly proposed settings of G_{max} and G_{mean}, which does offer more freedom in choosing the distance between the center of labeling and control conditions, i.e., it is not necessary to locate the untargeted arteries exactly at the center of the control condition, and the lowered visualization of PCA could be avoided by optimizing the width of the labeling condition. Another explanation could be that B_0 inhomogeneity could have caused a shift of the spatial distribution of the labeling/control pattern, which could also explain some of the asymmetry as observed in the in vivo plots of the spatial inversion profile (see Figure 8).

The second limitation is that only a straight artery was modelled in the simulation study and that performance of the newly proposed settings could be different for a tortuous artery. Although in the results of in vivo studies there was not any evident differences between the two newly proposed settings of G_{max} of 3.0 mT/m and 6.0 mT/m, a wider "w_{flow}" as produced by a low G_{max} (such as 2.0 or 3.0 mT/m) could result in a poorer inversion profile in a tortuous artery. This is similar for nonselective pCASL imaging and was, therefore, not considered the main goal of the current study, which focuses on the underlying mechanisms of how the shape of inversion profile is altered by the gradient parameters, which may help further protocol optimizations.

The third one is that, as also mentioned in the results section, some signal offsets and shifts in the inversion profile curves were observed in the in vivo study (Figure 8B), which could be attributed to the scanner drift across the scans and possible off-resonance effects. However, there were some more limitations when considering the experimental design: because of scan time restrictions, the inversion profile was obtained with a single average and at a short postlabeling delay, which means that the measured signal came from relatively large arteries rather than tissue, which caused some unwanted signal fluctuations. Moreover, the inversion profile curves obtained from two volunteers were not averaged to generate the mean inversion profile curve, because the distance between the right and left ICAs was not identical for these two volunteers. These limitations resulted in the rather noisy inversion profile curves, albeit confirming the general findings of the simulations.

Lastly, we only tested our optimized settings for ve-pCASL 4D-MRA in five healthy volunteers. In patient examinations, the occurrence of motion could be more frequent than in volunteer studies. Although the shorter scan time achieved by using our optimized settings could reduce the risk of motion occurrence, too narrow a labeling condition could reduce the labeling efficiency when motion occurs. Therefore, further optimization might be required for patient examinations.

5 | CONCLUSION

In summary, we have determined how changes in G_{max} and G_{mean} influence the spatial modulation of the inversion profile for vessel-encoded pCASL, with the specific goal in mind of allowing a faster acquisition for ve-pCASL 4D-MRA. A narrower labeling condition, larger and flatter control condition and sharper transition for the newly proposed settings were subsequently proven to allow 4D-MRA images of high quality in shorter scan time in the in vivo healthy volunteer study, and it was shown that the use of new settings lowered the risk of partial labeling of untargeted arteries.

ORCID

Yuriko Suzuki http://orcid.org/0000-0002-4851-7872
Thomas W. Okell http://orcid.org/0000-0001-8258-0659

REFERENCES

1. Jensen-Kondering U, Lindner T, van Osch MJ, Rohr A, Jansen O, Helle M. Superselective pseudo-continuous arterial spin labeling angiography. *Eur J Radiol*. 2015;84:1758–1767.
2. Fujima N, Osanai T, Shimizu Y, et al. Utility of noncontrast-enhanced time-resolved four-dimensional MR angiography with a vessel-selective technique for intracranial arteriovenous malformations. *J Magn Reson Imaging*. 2016;44:834–845.
3. Golay X, Petersen ET, Hui F. Pulsed star labeling of arterial regions (PULSAR): a robust regional perfusion technique for high field imaging. *Magn Reson Med*. 2005;53:15–21.
4. Hendrikse J, van der Grond J, Lu H, van Zijl PC, Golay X. Flow territory mapping of the cerebral arteries with regional perfusion MRI. *Stroke*. 2004;35:882–887.
5. Zimine I, Petersen ET, Golay X. Dual vessel arterial spin labeling scheme for regional perfusion imaging. *Magn Reson Med*. 2006;56:1140–1144.
6. Wong EC. Vessel-encoded arterial spin-labeling using pseudo-continuous tagging. *Magn Reson Med*. 2007;58:1086–1091.
7. Suzuki Y, Fujima N, Ogino T, et al. Acceleration of ASL-based time-resolved MR angiography by acquisition of control and labeled images in the same shot (ACTRESS). *Magn Reson Med*. 2018;79:224–233.
8. Berry ES, Jezzard P, Okell TW. An optimized encoding scheme for planning vessel-encoded pseudocontinuous arterial spin labeling. *Magn Reson Med*. 2015;74:1248–1256.
9. Wong EC, Guo J. Blind detection of vascular sources and territories using random vessel encoded arterial spin labeling. *MAGMA*. 2012;25:95–101.
10. Okell TW, Schmitt P, Bi X, et al. Optimization of 4D vessel-selective arterial spin labeling angiography using balanced steady-state free precession and vessel-encoding. *NMR Biomed*. 2016;29:776–786.
11. Chappell MA, Okell TW, Payne SJ, Jezzard P, Woolrich MW. A fast analysis method for non-invasive imaging of blood flow in individual cerebral arteries using vessel-encoded arterial spin labelling angiography. *Med Image Anal*. 2012;16:831–839.
12. Günther M. Efficient visualization of vascular territories in the human brain by cycled arterial spin labeling MRI. *Magn Reson Med*. 2006;56:671–675.
13. Okell TW, Chappell MA, Woolrich MW, Gunther M, Feinberg DA, Jezzard P. Vessel-encoded dynamic magnetic resonance angiography using arterial spin labeling. *Magn Reson Med*. 2010;64:430–438.
14. Chen JJ, Pike GB. Human whole blood T2 relaxometry at 3 Tesla. *Magn Reson Med*. 2009;61:249–254.
15. Ogg RJ, Kingsley PB, Taylor JS. WET, a T1- and B1-insensitive water-suppression method for in vivo localized 1H NMR spectroscopy. *J Magn Reson B*. 1994;104:1–10.
16. Okell TW, Chappell MA, Kelly ME, Jezzard P. Cerebral blood flow quantification using vessel-encoded arterial spin labeling. *J Cereb Blood Flow Metab*. 2013;33:1716–1724.
17. Sallustio F, Kern R, Gunther M, et al. Assessment of intracranial collateral flow by using dynamic arterial spin labeling MRA and transcranial color-coded duplex ultrasound. *Stroke*. 2008;39:1894–1897.

SUPPORTING INFORMATION

Additional Supporting Information may be found in the online version of this article.

FIGURE S1 Color-coded 2D maps of the simulated M_z as a function of distance in the direction of G_{xy} (left-right in these images) and in the flow-direction (bottom to top), with flow velocities of (A) 10 cm/s and (B) 50 cm/s. Red and blue colors show the uninverted and inverted magnetization, respectively. Only data simulated by unipolar approach is shown.

FIGURE S2 Color-coded 2D maps of the simulated M_z as a function of distance in the direction of G_{xy} (left-right in these images) and in the flow-direction (bottom to top), with G_{xy} to achieve a distance of (A) 50 mm which is approximate distance between right and left ICAs, and (B) 15 mm which is approximate anterior-posterior distance between ICAs and VAs, between the center of labeling and control conditions. Red and blue colors show the uninverted and inverted magnetization, respectively. Only data simulated by unipolar approach is shown.

FIGURE S3 Comparison of the simulated inversion profile curves (fixed G_{max} at 6.0 mT/m and variable G_{mean}) when using different pCASL flip angles and RF intervals: (A) the default setting with RF duration = 0.6 ms, RF interval = 1.0 ms, flip angle = 20º, (B) lower flip angle of 17º, (C) higher flip angle of 23º, and (D) longer RF duration of 1.2 ms.

FIGURE S4 Comparison of the simulated inversion profile curves (variable G_{max} and fixed G_{mean} at 0.2 mT/m) when using the different pCASL flip angles and RF interval: (A) the default setting with RF duration = 0.6 ms, RF interval

= 1.0 ms, flip angle = 20º, (B) lower flip angle of 17º, (C) higher flip angle of 23º, and (D) longer RF duration of 1.2 ms.

FIGURE S5 Representative ve-pCASL 4D-MRA images from one of the healthy volunteers.

FIGURE S6 ve-pCASL 4D-MRA images from all volunteers obtained from this study. Only representative single phase is shown.

How to cite this article: Suzuki Y, van Osch MJP, Fujima N, Okell TW. Optimization of the spatial modulation function of vessel-encoded pseudo-continuous arterial spin labeling and its application to dynamic angiography. *Magn Reson Med*. 2019;81: 410–423. https://doi.org/10.1002/mrm.27418